

Visualizing Small Objects Using Amplitude-Modulated Laser Light at Microwave Frequencies

Yuichiro Kogi ^{1,*}, Narumi Kimura ², Hiroyuki Ikezi ^{3,†}, Masaaki Inutake ⁴ and Atsushi Mase ³¹ Faculty of Engineering, Fukuoka Institute of Technology, Fukuoka 811-0295, Japan² Graduate School of Fukuoka Institute of Technology, Fukuoka 811-0295, Japan³ Global Innovation Center, Kyushu University, Kasuga 816-8580, Japan⁴ Department of Electrical Engineering, Graduate School of Engineering, Tohoku University, Sendai 980-8577, Japan

† Retired.

* Correspondence: kogi@fit.ac.jp; Tel.: +81-92-606-3599

Abstract: We reported on laboratory imaging experiments conducted using a system that utilizes amplitude-modulated infrared laser light at microwave frequencies. With modulations ranging from 11.1 to 15.1 GHz on a 1.55 μm near-infrared laser, the phase measurements of the modulation signals revealed a target shape with sub-mm precision. We also tested whether our system is able to achieve cross-range resolution in the spot-light mode synthetic aperture scheme. With the aid of “position-compensated signal processing”, synthetic aperture images were formed successfully. According to predications based on the principle of normal synthetic aperture radar, the spatial resolutions of the images were shown to be inversely proportional to the width of the collected data placed in the wavenumber space.

Citation: Kogi, Y.; Kimura, N.; Ikezi, H.; Inutake, M.; Mase, A. Visualizing Small Objects Using Amplitude-Modulated Laser Light at Microwave Frequencies. *A ppl. Sci.* **2022**, *12*, 9836. <https://doi.org/10.3390/app12199836>

Academic Editors: Santiago Royo and Mario De Cesare

Received: 12 July 2022

Accepted: 27 September 2022

Published: 29 September 2022

Publisher’s Note: MDPI stays neutral with regard to jurisdictional claims in published maps and institutional affiliations.



Copyright: © 2022 by the authors. Licensee MDPI, Basel, Switzerland. This article is an open access article distributed under the terms and conditions of the Creative Commons Attribution (CC BY) license (<https://creativecommons.org/licenses/by/4.0/>).

Keywords: remote sensing; LADAR; SAR; SAIL; imaging; AM laser; FM microwave

1. Introduction

Laser detection and ranging (LADAR) and synthetic aperture radar (SAR) are useful remote sensing devices and are used in many fields, such as military, agriculture, security, traffic, and disaster surveillance [1–5]. The wavelength and the bandwidth used in LADARs and SARs strongly affect the detectable range, spatial resolution, and back scattering cross-section of various targets; thus, measurement systems are designed to meet user demands in terms of detectable range and spatial resolution. This research was performed to verify whether a new approach, which is intended to be used in outdoor surveillance, could visualize a small target and extend the range and resolution of the measurable region.

In frequency-modulated (chirped) radars, data collection in the frequency domain enables synthetic aperture formation, allowing coherent radar data to be collected at multiple radar positions. Two-dimensional and three-dimensional images can then be obtained. Satellite and airborne synthetic aperture radars (SARs) are popular image collectors. The spatial resolution of a SAR is half a wavelength of the chirped frequency width in the range direction. The frequency chirp width is, however, limited by the allocated radar band width. In general, the allocated bandwidth for surveillance radar tends to be less than 1 GHz [6–8], while the range resolution of SARs is around 1 m. For monitoring the area suffering from disasters, radar must visualize various targets such as cars, rocks, trees, etc., on the ground. The size of these objects ranges from a few millimeters to a few meters. The present resolution around 1 m is not sufficient to identify these targets from the SAR image.

LADARs are distance measurement instruments that use short laser pulses, which are often used to measure elevation map on a terrain in the range under about 1 km [6]. Their current range resolution is typically 10 cm. Higher resolutions can be obtained using shorter laser pulses, but their use is limited by the requirement for detectable energy in pulses. Using phase coherence between laser pulses enhances scattered signal detection.

The modulation of laser light by chirped signals instead of short pulse modulations, which is also called LADAR, allows laser pulses that are many orders of magnitude larger [7]. In addition, the frequency chirp width is not limited by the radar frequency band allocation. This also helps to avoid the licensing requirements for radio wave emission. Some research using modulation laser for range measurement has been reported. A. Dorrington et al. [8] used a projection of a diverged amplitude modulated (AM) laser by a 100 MHz signal and a digital video camera with a heterodyne detection system. They demonstrated the visualization of a small target located at around a 5 m range with a range resolution of less than 1 mm within a measuring time of 10 s. W. Kim et al. [9] used the projection of a collimated comb pulsed laser using up to the 10th harmonic frequency component to extend the frequency bandwidth up to 10 GHz. They performed detailed research on ranging resolution using a corner cube reflector and showed a range resolution performance under 10 mm when the target range was around 2 m. S. Wheaton et al. [10] used the projection of diverged quadrature phase shift keying (QPSK) laser with 150 MHz signal and a digital camera. They showed a range resolution performance between 5 mm and 20 mm depending on the detected power under a measurement range of less than 1 m. E. Baumann et al. [11] used a collimated frequency modulated (FM) laser with a 1 THz modulation signal. They applied the system to small targets located under 10 m and demonstrated visualizing these targets with range resolution around few micrometers. These studies used amplitude, phase, pulse, and frequency modulation lasers to extend the bandwidth of the measurements to improve range resolution. These measurement instruments take two-dimensional or three-dimensional images like a snapshot camera when they collect data; that is, their measurement instruments take data by fixing a geometric relationship between the measurement instrument and targets. On that condition, cross-range resolution depends on the focal length of the focus lens used in the receiver and the range between the lens and targets, when an instrument employ diverged projection beam. When an instrument employs a collimated projection beam, cross-range resolution becomes the beam size on a target. In the far range measurement, cross-range resolution is limited by the real aperture of the receiver lens or collimation lens. In order to improve cross-range resolution even in the relatively far range, we aimed to develop the AM LADAR combined with the SAR, which is generally called synthetic aperture imaging LADAR (SAIL). In the SAIL measurement scheme, a measurement instrument collects back scattered light by moving its position, then performs synthetic aperture processing on the data to synthesize the large aperture. This synthetic aperture processing is explained in the following section. In principle, measurement using a large synthetic aperture enhances cross-range resolution. In our system, since laser light only works as a carrier for the microwave signals, all data processing methods are identical to those of microwave radars. An important difference between microwave and laser systems is how they are scattered when they reach the target surface. Since wave scattering occurs on surfaces with a roughness scale length that is larger than the wavelength, the surfaces that mirror-reflect the microwaves may scatter the laser light, in contrast to what takes place during mirror reflection. This results in there being significant differences in the image characteristics.

We have reported a LADAR experiment using a vector network analyzer (VNA) and an electro/optical (E/O) and optical/electro (O/E) transceiver, which was applied to the near-range (<10 m) small target to validate the measurement principle [7,12,13]. In this paper, we developed a LADAR system using a wide band microwave transmitter in place of the VNA [14]. This system change will be helpful during airborne LADAR measurements since the pulse repetition frequency (PRF) of the measurement will be over 100 times

faster than the VNA. We aim to visualize a small target, and to validate the replication of the LADAR experiment using a new transmitter system. This experiment is similar to the previous experiment reported in reference [8–11]. In addition to that, we also aim to visualize a small target by using spotlight-mode synthetic aperture imaging LADAR (SAIL) in lab experiments, and to validate the applicability of the developed system.

2. Data Processing Methods

Since laser light only works as a microwave signal carrier, signal processing is used to deal with the microwave signals. We consider a geometry in which a reference point set at the origin of the coordinate system, as shown in Figure 1.

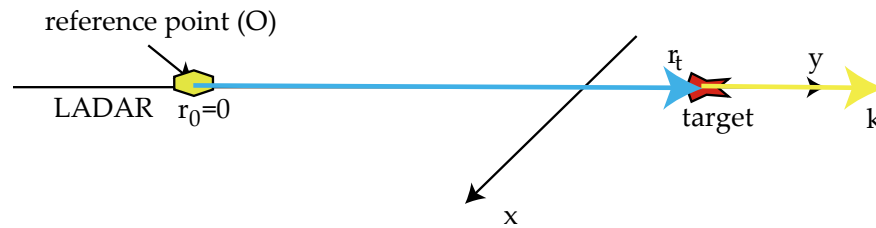


Figure 1. Coordinate system used for LADAR measurements.

The transmitter/receiver, TX/TR, position is at \mathbf{r}_0 , and the point target is at \mathbf{r}_t . The microwave-modulated laser light travels to the target over a distance of $|\mathbf{r}_0 - \mathbf{r}_t|$ and is scattered back to the transmitter/receiver. The scattered light signals are then detected and mixed with the reference microwaves, which have a waveform that is identical to the transmitted waveform. We chose to delay the reference signal by comparing the round-trip travel time to a reference, $2|\mathbf{r}_0| / c$. The interference signal is given by

$$\begin{aligned}
 F(k) &= A(\sigma) \exp[j2|k| \cdot (|\mathbf{r}_0 - \mathbf{r}_t| - |\mathbf{r}_0|)] \\
 &= A(\sigma) \exp[j2\mathbf{k} \cdot \mathbf{r}_t], \text{ for } |\mathbf{r}_t| \ll |\mathbf{r}_0|
 \end{aligned}
 \tag{1}$$

where $\mathbf{k} = (\omega/c) \cdot \mathbf{r}_t/|\mathbf{r}_t|$.

The amplitude depends on the target-scattering cross-section, σ .

In the experiment presented here, the laser light was spotted on a continuous surface. The system then detects the phase $\varphi = j2\mathbf{k} \cdot \mathbf{r}_t$. By scanning the focused spot, a 2D surface shape is found. The phase measurements have multiple-of- 2π ambiguity. If the microwave frequency is chirped and $F(\mathbf{k})$ is measured within a range of wavenumbers: from $\mathbf{k}_0 - \Delta\mathbf{k}/2$ to $\mathbf{k}_0 + \Delta\mathbf{k}/2$, then the Fourier transform of Equation (1) with respect to \mathbf{k} is

$$S(\mathbf{r}) = B(\sigma) \text{sinc}(\Delta\mathbf{k} \cdot (\mathbf{r} - \mathbf{r}_t)) \exp[j2\mathbf{k}_0 \cdot \mathbf{r}_t].
 \tag{2}$$

The peak position of the sinc function gives an approximate value of \mathbf{r} with the resolution $\pi/\Delta k$. Multiple-of- 2π ambiguity is reduced. Two-dimensional surface measurements allow phase unwrapping processing to avoid 2π ambiguity. In the LADAR experiment, we extracted the phase value at the maximum of the sinc function in Equation (2) to evaluate the range. It is also noted that the reference point employed in the LADAR experiment was set to the TX/RX position.

Due to space limitations in the laboratory, the SAIL experiments were set in a way in which small targets were on a rotatable stage instead of moving transmitter/receiver. We chose the reference point at the center of stage, as shown in Figure 2.

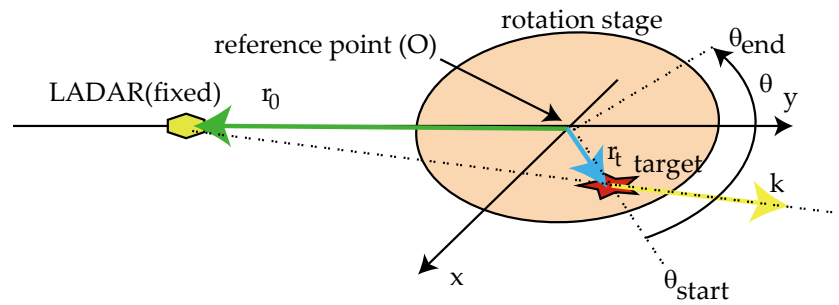


Figure 2. SALE measurement coordinate system.

On the coordinate system fixed onto the stage, the direction of k turns by $-\theta$ when the stage turns by θ . The $F(k)$ measurements are obtained by chirping the frequency, ω , and rotating the table; $F(k)$ is obtained from the area of k , $(k_0 - \frac{\Delta k}{2} < k < k_0 + \frac{\Delta k}{2}, \theta_{start} < \theta < \theta_{end})$. Interpolations of $F(k)$ data on to the rectangular coordinate system using $k_x = k \cos(\theta)$ and $k_y = k \sin(\theta)$ allow for the digital Fourier transform, FFT, of $F(k)$ to form 2D images. The $F(k)$ data are in a fan-shaped area with k_x and k_y spanning

$$K_x \sim k_0[\sin(\theta_{end}) - \sin(\theta_{start})]$$

$$K_y \sim k_0[1 - \cos(\theta_{start} \text{ or } \theta_{end})] + \Delta k. \tag{3}$$

The image widths of a point target are approximately π/K_x in the x direction and π/K_y in the y direction and can be much smaller than the width given by the frequency chirp width $\pi/\Delta k$.

3. Experimental Set-Up

3.1. LADAR System

Digital waveform synthesizers [14] generate identical waveforms of frequency-chirped microwaves repeatedly. The electro-optic modulator amplitude-modulated the laser light at the wavelength of 1.55 μm . The microwaves were frequency-chirped in the range of 11.1–15.1 GHz, which is much wider than the range allowed in the radar band. The chirped pulse width was typically 1.5 ms. The modulated light was amplified and sent out through a beam splitter, which consisted of a half mirror. The target-scattered lights went back to the same beam splitter and were detected, i.e., demodulated, to the microwave signals. Mixing with the delayed modulation microwaves resulted in complex coherent signals that were sampled to generate digital data.

In the first type of experiment (LADAR), the laser light was spotted on a metal sphere having diameter of $D = 94 \text{ mm}$ and that had been painted with retroreflective spray to increase its backward scattering power. The sphere surface scattered the laser light instead of mirror-reflecting. The spot position was scanned on the target in 2D by rotating the half mirror in the beam splitter. Here, 50 mm in horizontal and 50 mm in vertical area was scanned by 1 mm step, thus, there were 2500 measurement points. In this experiment, range was measured 100 times repeatedly at the same position to enhance the signal to noise ratio. Total measurement time was about 6 min. The size of the beam spot on the target was 7 mm. The range was set to 5.3 m. The set-up is depicted in Figure 3.

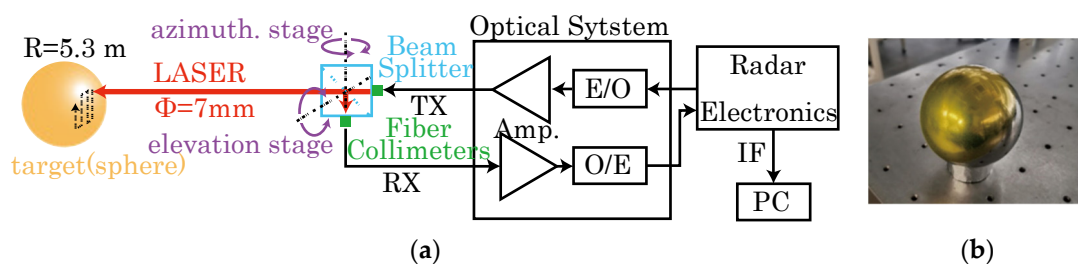


Figure 3. (a) Block diagram of the LADAR system. The laser, which is amplitude-modulated at the FM microwave frequencies, was spatially scanned on the surface of the target. (b) Picture of the spherical target with diameter of 94 mm, which was covered by reflective paint.

3.2. SAIL System

The second type of experiment was demonstration of synthetic aperture processing (SAIL). The target on the stage was rotated instead of rotating the beam splitter. The data were collected by rotating the rotation stage from -45 degree to $+45$ degree by 0.1 degree step. Here, 100 times measurements at each angle were performed for noise reduction. Total measurement time was about 3 min. The beam diameter at the target was enlarged to be larger than the rotating stage. Corner cube(s), which were placed on the rotating stage, were retroreflective point target(s). The setting is depicted in Figure 4.

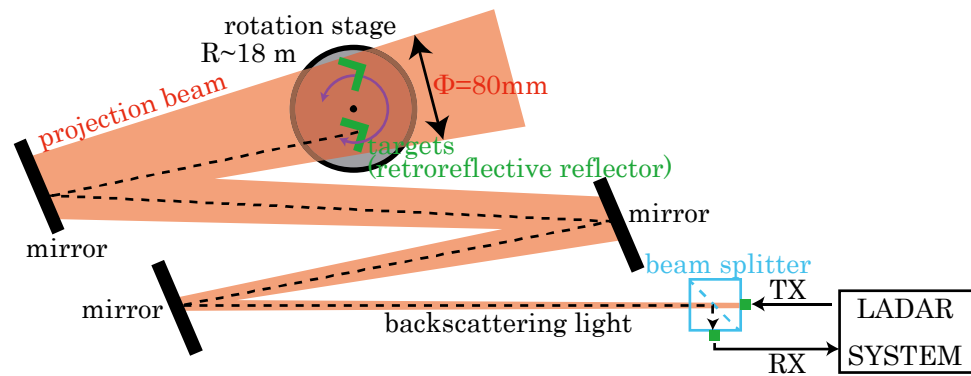
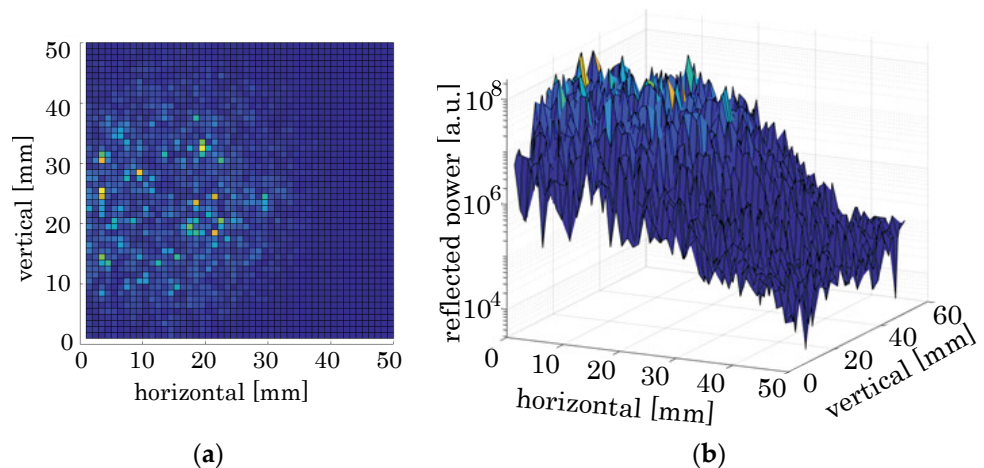


Figure 4. Top view of synthetic aperture experiment setup. The interference signals, $F(k)$, were collected as a function of the stage rotation angle and the chirped microwave frequency.

4. Experimental Results and Comparison between Two Experiments

4.1. Results of the LADAR Experiment

First, we describe the results that were obtained by the fixed-target-position measurements using the settings depicted in Figure 3a. The laser light was spotted on the sphere with a diameter of 94 mm. The spot size was 7 mm. Figure 5a, b shows that the scattered light from the front area within a diameter of 40 mm can be detected well. The scattered light intensity falls sharply outside of this area. The phases of the detected signals, φ , in the scanned area are shown in Figures 5c, d. The scattering point positions were found with the aid of $\varphi = j2k \cdot r_t$. We confirmed that the phase within the diameter of 40 mm showed a smooth decline. In Figure 6 the range, i.e., the position of the light scattering, is plotted by a blue line on the horizontal line that passes through the center of the sphere.



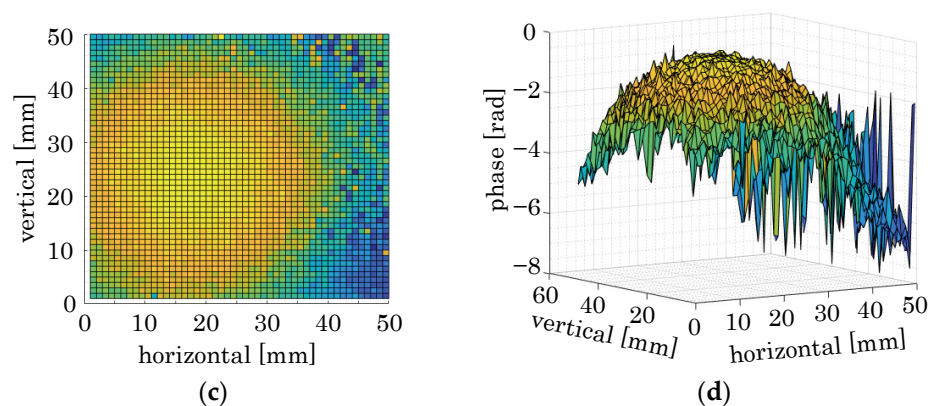


Figure 5. Image of the sphere obtained by the fixed target measurements: (a) the 2D amplitude image; (b) the 3D amplitude image; (c) the 2D phase image; (d) the 3D phase image.

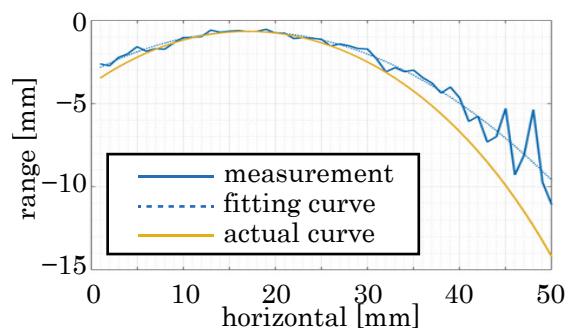


Figure 6. Range image of the sphere extracted on the horizontal axis from Figure 3b is plotted by thick blue curve. Blue dotted curve denotes the observed fitting curve. Orange curve denotes the actual shape of the sphere.

The blue dotted line and the yellow line denote the fitting curve using a quadratic function applied to the measurement results and real shape of the spherical target. The range values of the fitting and the real curves were almost consistent with each other within the 40 mm diameter. On the other side, the range value difference between them gradually increased toward the edge. We considered that this was caused by the finite spot size (7 mm) of the projection laser beam on the cross-range plane. The laser beam projected a small finite area on the target surface. In such a situation, the measured phase value is mainly considered to result from reflected waves with a large amplitude. Thus, the range measured with the phase likely corresponds to a target with a high backward cross-section in the projected area. Since the cross-section outside of the 40 mm diameter began to sharply decrease as shown in Figure 5b, phase values measured in the edge region would be strongly affected by the position closer to the center within the projected footprint of the laser. On the other side, the backward cross-section near center was almost flat, and average of the range inside the footprint was measured. Thus, from the measured cross-range error of the edge measurements, cross-range resolution was estimated to be about 7 mm, which is equal to the beam spot size. The measured range was fluctuating as shown in the blue solid curve in Figure 6. This fluctuation is dealt as a range resolution. The range resolution seemed to be depending on detected power at each measurement position, as studied in detail on the reference [10]. We did not perform detailed research on this relationship, however, brief analysis from Figures 5 and 6 was as follows. The signal to noise ratio (SNR) could be estimated from Figure 5b. The detected power level measured over 40 mm of the horizontal position did not change, thus, was thought to be a noise floor level. The SNR evaluated at 20 mm (center of the sphere), 35 mm, and 45 mm (edge) were over 100, 10, and 1, respectively. The range resolutions at corresponding

positions were about 0.2 mm, 1 mm, and 5 mm, respectively; which was improving as increasing in the SNR.

4.2. Results of the SAIL Experiment

The objects that were employed on the synthetic aperture measurements were chosen to be the optical corner cubes because both incident and reflected light travel along an identical path-length. Thus, an optical corner cube can be utilized as a point target, resulting in the reconstructed image of a point target becoming a point spread function (PSF). This is necessary to determine the spatial resolution. The interference data were obtained by turning the stage from $-\pi/4$ to $\pi/4$. The fan-shaped blue area in Figure 7 shows the wavenumber space where the interference data were taken. To obtain the image, Fourier transform was carried-out in the red area [15].

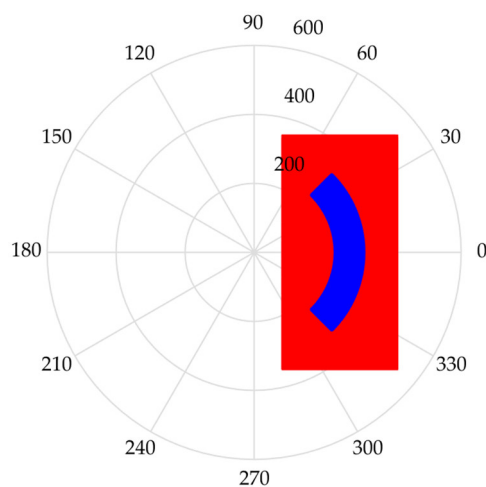


Figure 7. The wavenumber k space showing the area where the interference data were taken (blue) and where 2D FFT was performed (red). This polar graph was plotted as a function of the azimuth look angle in degree and wavenumber of the FM microwave in rad/m. The azimuth look angle corresponds to the angle of the rotation stage.

In Figure 8a, the positions of two corner cubes are separated by 110 mm. The photograph in Figure 8b corresponds to the image in Figure 8a. Both corner cubes were located at the same radius. In Figure 8c, the corner cubes positions are diagonal, separated by a cross-range of 53 mm in and by 40 mm in the range directions, as shown in the photograph Figure 8d. The observed separation between the two targets were in agreement with the set positions. The image width at half height in the cross-range direction was found to be about 9 mm and about 24 mm in the range direction. The observed widths showed approximate agreement with π/K_x and π/K_y , as shown in Equation (3); that is, the expected image resolutions in cross-range and range directions are about 8 mm and 37.5 mm, respectively.

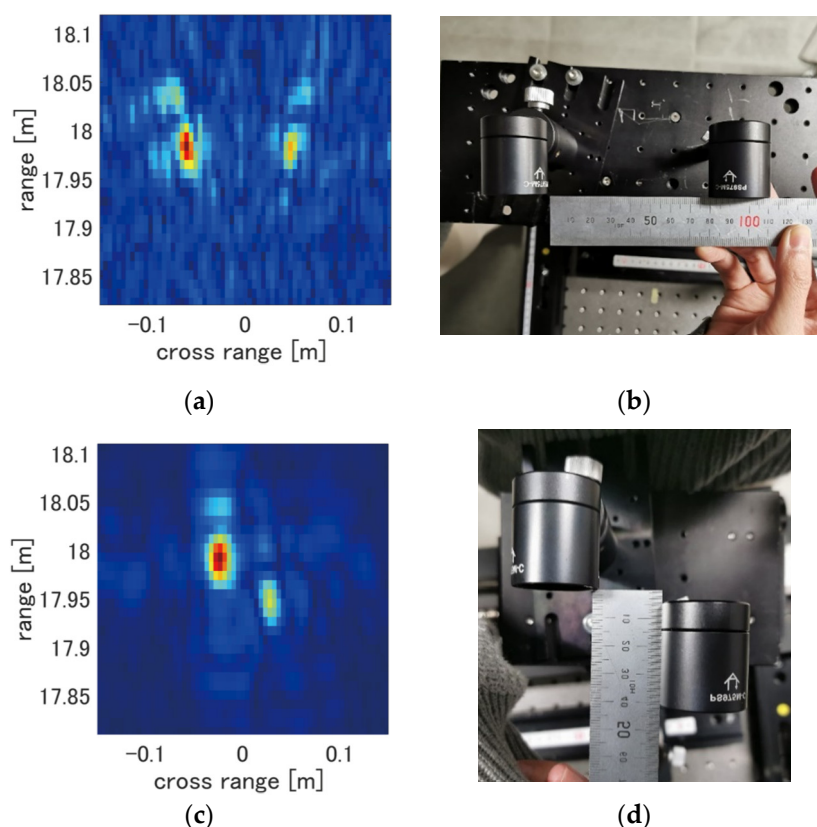


Figure 8. Synthetic images of two corner cube targets (a,c) and corresponding photographs of the targets (b,d). The two reflectors are separated by 110 mm in the cross-range direction; (a,b) diagonal separation of 53 mm in cross-range and in-range separation of 40 mm (b,d).

4.3. Comparison between the LADAR and the SAIL Results

We applied two types of imaging systems to the targets and acquired good images successfully. Here, we discuss the advantages and disadvantages of these two diagnostics and suitable experimental situations for each diagnostic in terms of the measurable range and analysis difficulty.

Firstly, since our SAIL system employed the ISAR technique—i.e., the targets were moved instead of the LADAR—this system can only observe moving targets. In addition to this disadvantage, this system requires that the positions of the moving targets at each measurement be pre-known when used with the present analysis method. A reconstruction method that does not need to know the target position in advance needs to be developed in future research. However, the LADAR can be applied to both moving and stationary targets. As this system needs to scan the beam spatially, moving targets must stay in the same position during the scan. In the present system, the scan speed was very slow since an electrically controlled stepping motor was utilized.

Secondly, a suitable target range between these diagnostics is considered to be around 1000 m in terms of the cross-range resolution. For the fine cross-range resolution, the LADAR system requires that the projection beam have a spot size in the target range that is as small as possible. Nevertheless, a transmitter with a large aperture is utilized, and the spot size with range of over 1000 m becomes over few centimeters in size. However, the SAIL system does not require a collimated projection beam, but it does require a wide azimuth look angle to improve the cross-range resolution; that is, SAIL requires a diverged projection beam. In general engineering and developing a diverged projection beam is easier than collimation. However, since a diverged projection beam indicates a low-gain transmitter, the reflection power from the target will often fall below noise level in this case. To achieve a well-resolved and high-contrast image, even when utilizing a

low-gain transmitter, the IF data taken by each repetition measurement must be well correlated before the Fourier transformation process is applied. In order to achieve that, the precise estimation of the target positions is a key issue that will be researched in the near future.

5. Conclusions

We applied LADAR and spotlight-mode SAIL, both of which employed an amplitude-modulated laser at microwave frequencies, to validate this methodology by visualizing small targets. For resolution improvement, we substituted the infrared laser for microwaves as a carrier of the modulation signal in order to utilize a wider bandwidth (4 GHz), which is difficult to permit a license in the microwave band. It was confirmed that the LADAR employing a new FM transmitter module could visualize the target shape with range and cross-range resolutions of under 1 mm and 7 mm, which are consistent with our previous LADAR system utilizing a VNA. The spotlight-mode SAIL system and image formations were demonstrated for the first time. The range and cross-range resolutions of this system were found to be about 24 mm and 9 mm, respectively. These spatial resolutions were in good agreement with those predicted by the measurement principle: 37.5 mm and 8 mm, respectively. On microwave SARs, it is difficult to improve the spatial resolution by collecting data on a wider wavenumber area since the scattering cross section of an object will vary both in the incident angle and frequency. Our method utilizes a fixed wavelength laser as a probing beam, with scattering response possibly becoming more simple compared to that of microwaves. This issue will be evaluated in future experiments. From the comparison between these two measurement results, we can conclude that LADAR is advantageous when making measurements in a range that is shorter than 1000 m due to the cross-range resolution as well as when taking stationary target measurements. On the other hand, SAIL with the spot-light mode inverse SAR technique was thought to be advantageous when making longer-range measurements and moving-target measurements. However, these difficulties such as low-amplitude signals and the requirement of knowing the precise target position must be solved by analysis techniques in the future.

6. Patents

This research is published as the following patent:

“Laser Radar and Synthetic Aperture Laser Radar Devices”, M. Inutake, H. Ikezi, A. Mase, Y. Kogi, and M. Sato, JP 2015-5686342.

Author Contributions: Data curation, N.K.; Formal analysis, Y.K. and H.I.; Funding acquisition, Y.K., M.I. and A.M.; Investigation, N.K., H.I. and A.M.; Methodology, H.I.; Project administration, Y.K., M.I. and A.M.; Writing—original draft, Y.K.; Writing—review & editing, H.I. All authors have read and agreed to the published version of the manuscript.

Funding: This work was supported by JSPS KAKENHI grant numbers 26289126 and 15K14005. Part of this work was carried out under the Cooperative Research Project Program of the Research Institute of Electrical Communication, Tohoku University.

Informed Consent Statement: Not applicable.

Data Availability Statement: The data presented in this study are available on request from the corresponding author. The data are not publicly available due to unformatted primitive data.

Conflicts of Interest: The authors declare no conflicts of interest.

References

1. Balenzano, A.; Mattia, F.; Satalino, G.; Davidson, M.W. Dense Temporal Series of C-and L-Band SAR Data for Soil Moisture Retrieval over Agricultural Crops. *IEEE J. Sel. Top. Appl. Earth Obs. Remote Sens.* **2010**, *4*, 439–450.
2. Eldhuset, K. An Automatic Ship and Ship Wake Detection System for Spaceborne SAR Images in Coastal Regions. *IEEE Trans. Geosci. Remote Sens.* **1996**, *34*, 1010–1019. <https://doi.org/10.1109/36.508418>.
3. Navarro-Serment, L.E.; Mertz, C.; Vandapel, N.; Hebert, M. LADAR-Based Pedestrian Detection and Tracking. 2008. Available online: https://kilthub.cmu.edu/articles/LADARbased_Pedestrian_Detection_and_Tracking/6555293/files/12037529.pdf (accessed on 7 June 2022).
4. Hinz, S.; Meyer, F.; Eineder, M.; Bamler, R. Traffic Monitoring with Spaceborne SAR—Theory, Simulations, and Experiments. *Comput. Vis. Image Underst.* **2007**, *106*, 231–244. <https://doi.org/10.1016/j.cviu.2006.09.008>.
5. Kogi, Y.; Ikezi, H.; Mase, A.; Ito, N.; Sato, M.; Suzuki, A.; Sakai, F.; Mizukami, S.; Kamewari, K.; Inutake, M. Development of Spotlight Mode SAR “Live SAR” for Flood Area Surveillance. In Proceedings of the Conference Proceedings of 2013 Asia-Pacific Conference on Synthetic Aperture Radar (APSAR), Tsukuba, Japan, 23–27 September 2013; pp. 257–260.
6. McManamon, P.F. Review of Ladar: A Historic, yet Emerging, Sensor Technology with Rich Phenomenology. *Opt. Eng.* **2012**, *51*, 14.
7. Mase, A.; Kogi, Y.; Kuwahara, D.; Nagayama, Y.; Ito, N.; Maruyama, T.; Ikezi, H.; Wang, X.; Inutake, M.; Tokuzawa, T.; et al. Development and Application of Radar Reflectometer Using Micro to Infrared Waves. *Adv. Phys. X* **2018**, *3*, 1472529. <https://doi.org/10.1080/23746149.2018.1472529>.
8. Dorrington, A.A.; Cree, M.J.; Payne, A.D.; Conroy, R.M.; Carnegie, D.A. Achieving Sub-Millimetre Precision with a Solid-State Full-Field Heterodyning Range Imaging Camera. *Meas. Sci. Technol.* **2007**, *18*, 2809. <https://doi.org/10.1088/0957-0233/18/9/010>.
9. Kim, W.; Fu, H.; Lee, K.; Han, S.; Jang, Y.-S.; Kim, S.-W. Photonic Microwave Distance Interferometry Using a Mode-Locked Laser with Systematic Error Correction. *Appl. Sci.* **2020**, *10*, 7649. <https://doi.org/10.3390/app10217649>.
10. Wheaton, S.; Bonakdar, A.; Nia, I.H.; Tan, C.L.; Fathipour, V.; Mohseni, H. Open Architecture Time of Flight 3D SWIR Camera Operating at 150 MHz Modulation Frequency. *Opt. Express* **2017**, *25*, 19291–19297. <https://doi.org/10.1364/OE.25.019291>.
11. Baumann, E.; Giorgetta, F.R.; Deschênes, J.-D.; Swann, W.C.; Coddington, I.; Newbury, N.R. Comb-Calibrated Laser Ranging for Three-Dimensional Surface Profiling with Micrometer-Level Precision at a Distance. *Opt. Express* **2014**, *22*, 24914–24928. <https://doi.org/10.1364/OE.22.024914>.
12. Wang, X.; Mase, A.; Ikezi, H.; Inutake, M.; Kogi, Y.; Uchino, K. Synthetic Aperture Radar Using Ultra-Wideband Microwave-Modulated Laser. *J. Electromagn. Waves Appl.* **2014**, *28*, 1275–1281. <https://doi.org/10.1080/09205071.2014.917994>.
13. Mase, A.; Kogi, Y.; Ikezi, H.; Inutake, M.; Wang, X. Study of Imaging Radar Using Ultra-Wideband Microwave-Modulated Infrared Laser. In *Infrared Remote Sensing and Instrumentation XXIV*; SPIE: Bellingham, WA, USA, 2016; Volume 9973, pp. 127–132.
14. Kimura, N.; Kogi, Y.; Mase, A.; Ikezi, H.; Inutake, M. Throughput Improvement and Evaluation of a Laser Radar with a High-Speed Sweep Oscillator. In Proceedings of the 2020 6th International Conference on Engineering, Applied Sciences and Technology (ICEAST), Chiang Mai, Thailand, 1–4 July 2020; pp. 1–4.
15. Jackowatz, C.; Wahl, D.; Eichel, P.; Ghiglia, D.; Thompson, P. *Spotlight-Mode Synthetic Aperture Radar: A Signal Processing Approach*; Springer: Berlin/Heidelberg, Germany, 1996; ISBN 0-7923-9677-4.